processes

MDPI

Technical Note

TBM Rapid Tunneling Roadway Support Parameters Design and Process Research

Tao Hou [1], Zhonghui Xie [1], Ling Zhang [1], Guogang Cui [1], Ziwei Ding [2,*], Huafu Qiu [2] and Yuhang Li [2]

[1] Shaanxi Zhengtong Coal Industry Co., Ltd., Xianyang 713600, China; houtaoztmy@163.com (T.H.); xiezhonghuiztmy@163.com (Z.X.); zhanglingztmy@163.com (L.Z.); cuiguogangztmy@163.com (G.C.)
[2] School of Energy Engineering, Xi'an University of Science and Technology, Xi'an 710054, China; huafuqiu@xust.edu.cn (H.Q.); 22203226069@stu.xust.edu.cn (Y.L.)
* Correspondence: zwding@xust.edu.cn

Abstract: Taking the specific production geological conditions of the auxiliary transportation lane in the west area of Gaojiabao coal mine of Shaanxi Zhengtong Coal Industry as the research background, based on the anchorage support theory and the characteristics of the TBM digging process, numerical simulation, theoretical analysis, and other research methods were used to investigate the depth of the destruction of the plastic zone of the surrounding rock of the roadway to form the reasonable support parameters of a large cross-section of hard rock roadway suitable for TBM digging and to propose an intelligent digging and support process of the TBM corresponding to the on-site practice. The proposed intelligent tunneling support technology corresponds to a field practice of TBM. The study shows that: combined with the field industrial test and adjusted by the peripheral rock deformation and damage law, the anchor diameter of 20 mm, the length of 2500 mm left-hand threaded steel anchors, row spacing of 1100 mm, spacing of 1200 mm, and the anchor diameter of Φ21.8 mm, the length of 6200 mm left-handed threaded steel anchors, row spacing of 1100 mm, spacing of 1200 mm are the most reasonable solutions, which can ensure the control of the tunnel peripheral rock. The program is the most economically efficient in ensuring the control of deformation of the roadway perimeter rock and maintaining normal use.

Keywords: rapid tunneling; surrounding rock deformation; roadway support scheme; parameter design; tunneling process optimization

Citation: Hou, T.; Xie, Z.; Zhang, L.; Cui, G.; Ding, Z.; Qiu, H.; Li, Y. TBM Rapid Tunneling Roadway Support Parameters Design and Process Research. *Processes* **2023**, *11*, 2708. https://doi.org/10.3390/pr11092708

Academic Editors: Hongxiang Xu, Gan Cheng, Guixia Fan and Carlos Sierra Fernández

Received: 18 August 2023
Revised: 5 September 2023
Accepted: 8 September 2023
Published: 11 September 2023

1. Introduction

In recent years, tunnel boring machines (TBMs), the most advanced tunnel digging machines in the world [1–6], have gradually started to be widely used in coal mine engineering construction [7–16]. They can satisfy the simultaneous operation of multiple processes, such as excavation, slag discharge and support, and have many advantages such as fast excavation speed, good forming quality, safety and environmental protection. With the extension of mining depth, the variety of minerals underground becomes more abundant [17–19], the safety risk of the mining area is greatly improved [20] and its mining conditions are complicated, which further limit the tunneling efficiency, and reasonable tunnel support parameters and reliable support technology are necessary to achieve safe and efficient production in mines. Domestic scholars have analyzed and researched the optimal design of roadway support schemes and support parameters using methods such as theoretical analysis and numerical simulation based on the analysis of roadway characteristics [21–30]. More scholars have researched the TBM rapid excavation support process to effectively improve the working face excavation efficiency and ensure the safe and rapid excavation of the roadway [31–38].

The application of TBMs in coal mine engineering is becoming increasingly widespread, especially in coal mine shaft engineering projects, which have gained a large number of successful applications. Nowadays, China is the country with the largest scale and number of

tunnels and underground projects, the most complex geological conditions and structures, and the fastest development of construction technology in the world. However, most mine tunnels have been supported by anchoring technology, and the support parameters are often copied from other mines or tunnels, which lack a scientific basis. Based on previous research, the author analyzed and designed the roadway support parameters using various research methods, such as numerical simulation and theoretical analysis based on the theory of anchorage support and the characteristics of the TBM boring process. Its practical application can effectively alleviate coal mine mining succession problems, and it also has very important reference value for the research of rapid rock tunneling technology under similar conditions.

2. Project Overview

Shaanxi Zhengtong Coal Gaojiabao coal mine is located in the northwest of the Binchang mine area, with a well field area of 219 square kilometers, a mine reserve of 974 million tons, a designed recoverable reserve of 470 million tons, a service life of 62.5 years, a designed production capacity of 5.0 Mt/a, a main mining Yan'an Group 4 coal seam with a burial depth of 1000~1100 m, and a roadway layout as shown in Figure 1. The average burial depth of the auxiliary transportation road in the west area of the Gaojiabao coal mine is over 900 m, and the dug section is a circular section with a net diameter of 6.5 m and a net section area of 33.17 m^2, as shown in Figure 2. The total length of the roadway is 6500 m, and the maximum slope is 6°. According to the design of the auxiliary transportation roadway in the west area, three layers of rock need to be crossed during the roadway boring process, which are 4 coal, mudstone and medium-grained sandstone. The position relationship of the three layers is shown in Figure 3, and the physical and mechanical parameters of each rock layer are shown in Table 1.

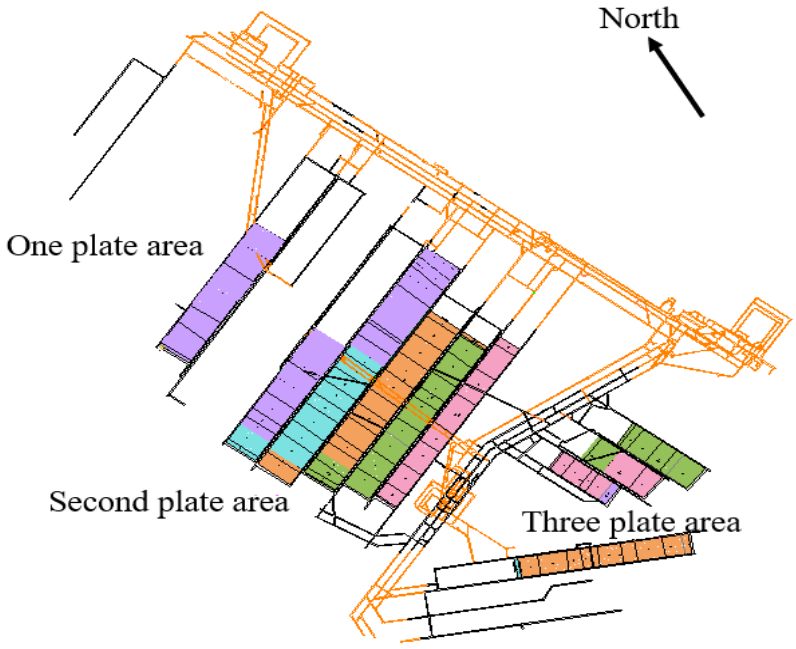

Figure 1. Schematic layout of the tunnel.

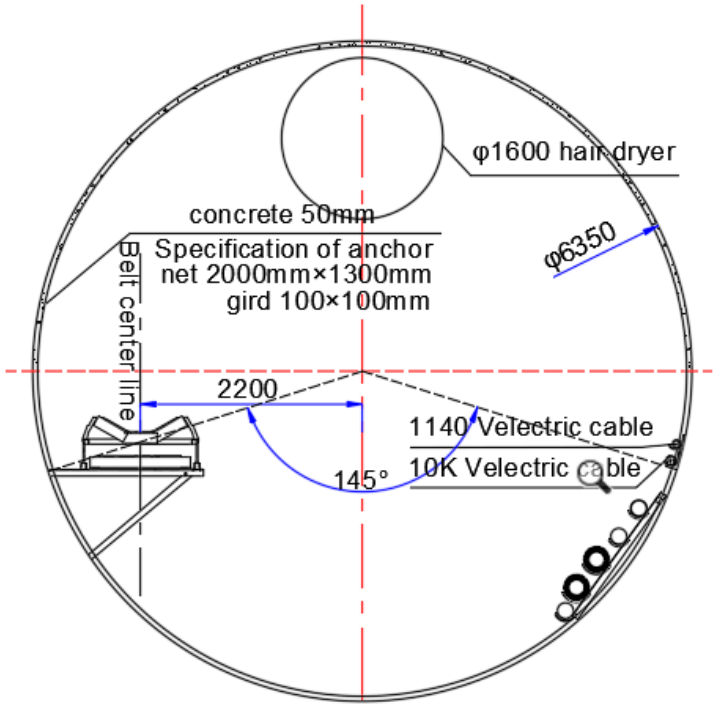

Figure 2. TBM roadway tunneling cross-section.

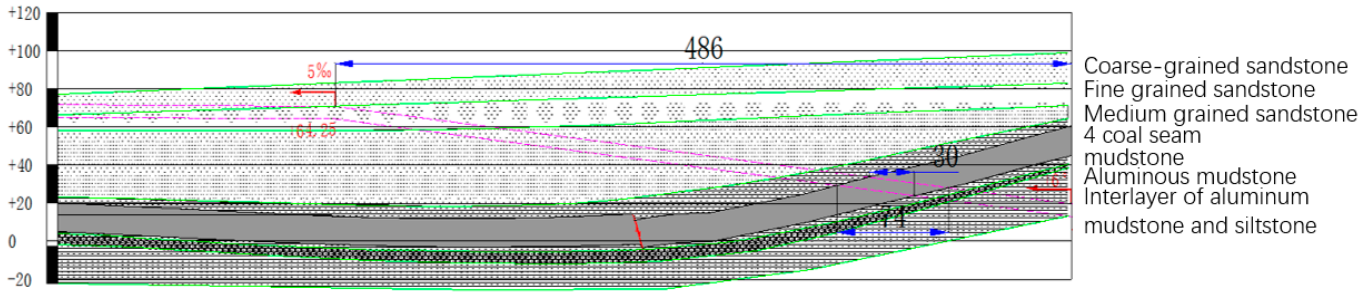

Figure 3. Schematic diagram of the rock position relationship.

Table 1. Mechanical parameters of each stratum.

Rockiness	Thickness /m	Density/ (kg/m^3)	Bulk Modulus/GPa	Shear Modulus/GPa	Angle of Internal Friction/°	Internal Cohesion/MPa	Tensile Strength/MPa
Medium-grained sandstone	25	251.02	1.41	1.01	39.11	2.69	1.22
Mudstone	3	248.98	1.01	0.69	38.77	3.78	1.70
4 Coal seam	15	1470	5.55	0.82	33.5	3.8	2.24

Steps in the tunneling machine's operation: start the digging cycle; reset and brace the support system; adjust the orientation and attitude of the TBM; connect the cutter shield with the rock to support the surrounding rock; rotate the cutter, and start the propulsion cylinder to advance to the cutter; in the process of the cutter's advancement, carry out other auxiliary operations in parallel; at the end of the advancement stroke, stop the cutter's rotation; change the step, and adjust the orientation and attitude of the TBM; and start a new cycle of digging.

3. Mechanical Model and Calculation of the Plastic Zone of the Tunnel Surrounding Rock

3.1. Mechanical Mechanism of the Formation of the Plastic Zone in the Tunnel Surrounding Rock

3.1.1. Mechanical Model of Circular Roadway Enclosure under Nonisobaric Conditions

The circular roadway mechanics model is somewhat simplified by considering it as an isotropic homogeneous medium. Given that the radius of the roadway is much smaller than the burial depth of the roadway and the length of the roadway alignment is generally larger, the surrounding rock stress is assumed to be in a uniform load state and is transformed into plane strain for analysis. The simplified mechanical model of the circular roadway is shown in Figure 4.

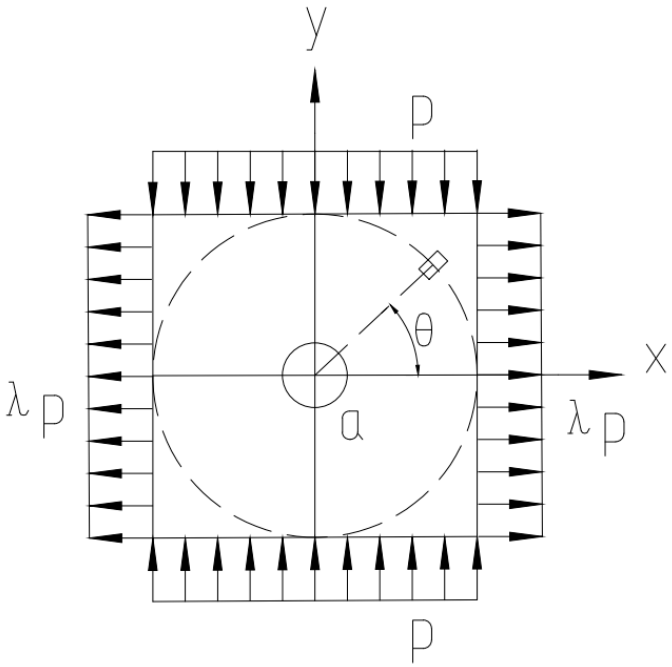

Figure 4. Bidirectional unequal pressure circular roadway mechanics model.

Using the two-dimensional stress distribution solution around the circular hole in the elastic plate in elastodynamics, the stress solution at a point of the roadway envelope under two-way unequal compressive stress conditions can be obtained as follows:

$$\begin{cases} \sigma_\gamma = \frac{P}{2}\left[(1+\lambda)\left(1-\frac{\alpha^2}{\gamma^2}\right)+(1-\lambda)\left(1-4\frac{\alpha^2}{\gamma^2}+3\frac{\alpha^4}{\gamma^4}\right)\sin 2\theta\right] \\ \sigma_\theta = \frac{P}{2}\left[(1+\lambda)\left(1-\frac{\alpha^2}{\gamma^2}\right)-(\lambda-1)\left(1+3\frac{\alpha^4}{\gamma^4}\right)\cos 2\theta\right] \\ \tau_{\gamma\theta} = \frac{P}{2}\left[(1-\lambda)\left(1+2\frac{\alpha^2}{\gamma^2}\right)\right] \end{cases} \quad (1)$$

where σ_r is the radial stress, MPa; σ_θ is the annular stress, MPa; $\tau_{r\theta}$ is the tangential stress, MPa; λ is the lateral pressure coefficient; and r and θ are the pole radius and pole angle.

3.1.2. Calculation of Plastic Boundary of Circular Roadway Enclosure under Nonisobaric Conditions

Using the Moore–Cullen criterion [39], the following conditions can be obtained for the stress in the plastic zone of the roadway envelope:

$$sin\varphi = \frac{\sqrt{(\sigma_\theta-\sigma_r)^2+4\tau^2{}_{r\theta}}}{\sigma_\theta+\sigma_r+2c\ cos\varphi} \quad (2)$$

Let the plastic zone boundary be r_p; then, on the elastic–plastic zone boundary with $r = r_p$, the surrounding rock stress should satisfy both conditions of Equations (1) and (2). Therefore, by associating Equation (1) with Equation (2), we obtain the implicit equation of the plastic boundary r_p of the circular tunnel surrounding rock on θ under the condition of a nonuniform stress field:

$$cos^2(2\theta) + \frac{2}{\omega}\left[\frac{1+\lambda}{4(1-\lambda)}\left(1-2\alpha^2+3\alpha^4\right) - \frac{\left(1+\lambda+\frac{2c\ cot\varphi}{p}\right)}{2(1-\lambda)}\right]cos2\theta - \frac{1}{\omega}\left[\frac{(1+\lambda)^2\alpha^2}{4(1-\lambda)^2} + \frac{\left(1+2\alpha^2-3\alpha^4\right)}{4\alpha^2} + \frac{\left(1+\lambda+\frac{2c\ cot\varphi}{p}\right)sin^2\varphi}{4\alpha^2(1-\lambda)^2}\right] = 0 \quad (3)$$

where $\omega = \alpha^2 sin^2\varphi + 2 - 3\alpha^2$; $\alpha = \frac{a}{r_p}$; c is the cohesion of the surrounding rock; φ is the internal friction angle of the surrounding rock; r_p is the radial plastic zone boundary; a is the radius of the circular roadway; and p is the stress.

3.2. Plastic Damage Characteristics of the Roadway Surrounding Rock under Different Lateral Pressure Coefficients

According to the invisible equation of Equation (3), the numerical calculation method was used to calculate the plastic zone of the sandstone tunnel enclosing rock under different lateral pressure coefficients, and the safety coefficient was taken as 0.8, so that the range of the plastic zone of the tunnel enclosing rock under different horizontal stresses (lateral pressure coefficients) was obtained, which is shown in Figure 5. As the lateral pressure coefficient increases, the plastic zone of the surrounding rocks of the two sides of the roadway decreases, and the plastic zone of the surrounding rocks of the roof of the roadway slowly increases. When the lateral pressure coefficient of the surrounding rocks of the roadway is 1.8, the plastic zone of the roof of the roadway reaches 0.75 m, and when the lateral pressure coefficient is greater than 1.8, the left side boundary of the plastic zone of the surrounding rocks of the roadway starts to become blurred.

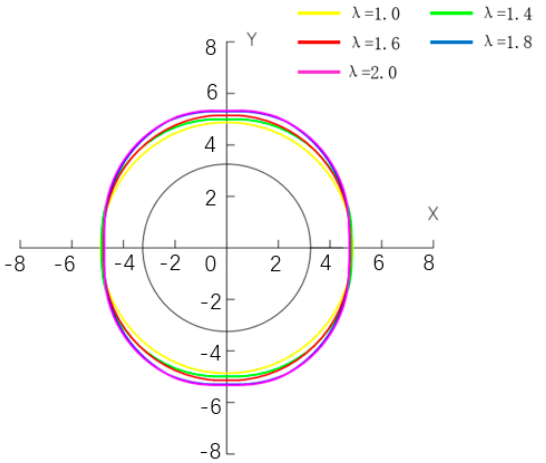

Figure 5. Plasticity zone of the tunnel surrounding rock under different lateral pressure coefficients.

3.3. Distribution Characteristics of the Plastic Zone of the Tunnel Surroundings under Different Lithological Conditions

According to the measured ground stress distribution, the plastic zone calculation parameters are shown in Table 2 using the numerical calculation method, and the range of the plastic zone morphology of the tunnel surrounding rock is obtained. The results are shown in Figure 6.

Table 2. Calculated parameters of the plastic zone in the different lithological layers.

Rockiness	Depth of Burial	Weight Capacity	Roadway Radius	Angle of Internal Friction	Internal Cohesion	Lateral Pressure Coefficient
4 Coal	935	14,060	3.25	33.5	3,800,000	1.8
Mudstone	925	24,400	3.25	38.77	3,780,000	1.8
Medium-grained sandstone	915	24,600	3.25	39.11	2,690,000	1.8

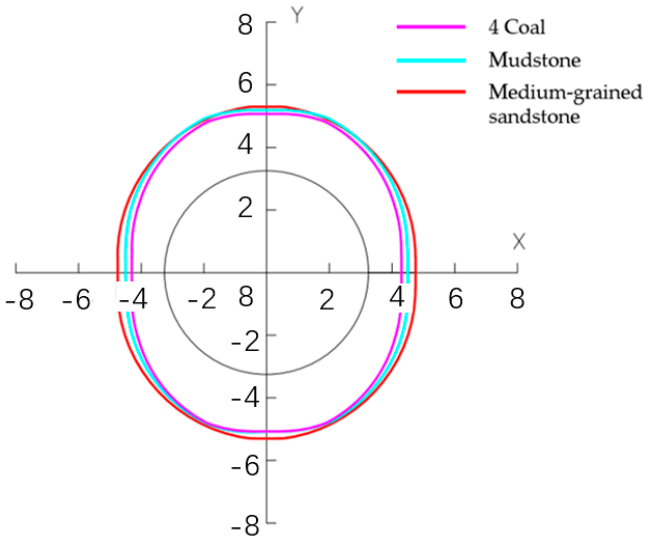

Figure 6. Calculated results of the plastic zone in the different lithological layers.

The calculated results show that under the condition of a lateral pressure coefficient of 1.8, the range of plastic zone in the vertical direction of the roadway is obviously larger than that in the horizontal direction. In different types of rock formations, under different conditions of surrounding rock strength, the range of the plastic zone of the surrounding rock in the top and bottom slabs of the roadway does not change obviously, and the range of the plastic zone of the surrounding rock in the two helpers of the roadway changes obviously. With an increase in the rock strength, the range of its plastic zone decreases. The medium-grained sandstone has the smallest strength, and its plastic zone range is the largest; 4 coal has the largest strength, and its plastic zone range is the smallest.

4. Intelligent TBM Tunneling Roadway Support Design

4.1. Theoretical Basis for Roadway Support Design

4.1.1. Calculation of Anchor Length Based on Suspension Theory

$$L \geq L_1 + L_2 + L_3 \tag{4}$$

where L is the total length of the anchor rod, m; L_1 is the exposed length of the anchor rod (including the thickness of steel belt, pallet, and nut), 0.1 m; L_2 is the effective length (the top anchor rod takes L_2 as the height of the fall of the loose ring of surrounding rock b; the side anchor takes the L_2 as the depth of side crushing c), 2.1 m; and L_3 is the depth of the anchor into the rock layer, a fixed value of 0.2 m.

In this case, the height of the perimeter rock loosening and bubbling b and the depth of side crushing c are, respectively:

$$\mathrm{b} = \frac{\frac{B}{2} + H\tan\left(45^\circ - \frac{w}{2}\right)}{f}$$
$$\mathrm{c} = H\tan\left(45^\circ - \frac{w}{2}\right)$$

where B is the horizontal width, and H is the horizontal height.

Substitute the above parameters into Equation (4) for the calculation, and the anchor length is 2.4 m.

4.1.2. Distance between Rows of Anchor Rods

It should meet:

$$a < \sqrt{\frac{G}{kL_2\gamma}} \tag{5}$$

where a is the anchor rod (cable) between the row distance, m; G is the anchor rod design anchorage force, 150 KN per root; k is the safety factor, generally 2; L_2 is the effective length (top anchor rod takes b; help takes c), 2.1 m; γ is the rock volume weight (weighted average), 25.48 KN/m^3 [40,41].

Substitute the above parameters into Equation (5) to get a 1.18 m.

4.1.3. Calculation of Anchor Cable Length According to Suspension Theory

$$L = KH + L_1 + L_2 \tag{6}$$

$$H = \frac{B}{2f} \tag{7}$$

where L is the length of the anchor cable, m; H is the height of the riser arch, m; K is the safety factor, generally 2; L_1 is the depth of the anchor cable anchored into stable rock, 0.4 m; L_2 is the exposed length of the anchor cable in the roadway, 0.2 m; B is the width of the roadway excavation, 6.5; f is the rock solidity factor, 1.5 [40,41].

Substitute the above parameters into Equations (6) and (7) to calculate L as 4.80 m.

4.1.4. Anchor Cable Spacing and Row Distance Calculation

This is usually calculated by equal spacings between anchor rows, taking a:

$$a = \sqrt{Q/(KHr)} \tag{8}$$

where a is the distance between rows of anchor ropes; Q is the design anchoring force of anchor ropes, 250 KN per root; H is the height of riser arch, take 2.1 m; r is the gravity density of suspended sandstone, 25.48 KN/m^3; K is the safety factor, generally 2 [40,41].

Substitute the above parameters into Equation (8) to obtain 1.53 m.

According to the above calculations, the design anchor parameters are as follows: anchor rod diameter is 20 mm; left-hand threaded-steel anchor rod length is 2500 mm, row distance is 1100 mm, spacing is 1200 mm, anchor cable diameter is Φ21.8 mm, length of left-hand threaded steel anchor rod is 6200 mm, row distance is 1100 mm, and spacing is 1200 mm, which meet the support requirements.

4.2. Roadway Support Design

The roadway anchor rods have the following characteristics: left-handed, longitudinal, reinforcement-free, high-strength rebar anchor rods, rectangular arrangement, 10 rows each, each anchor rod is anchored with 2 MSK2850 resin anchoring agent, Stick the anchoring agent into the stable rock stratum, dip the anchoring agent on the outside with a tray, and then tighten it, the tray must be close to the rock surface.

The anchor ropes are made of steel stranded anchor ropes, 9 per row, with alternate arrangement of anchor ropes and anchor rods; two anchor ropes per anchor beam, with anchor ropes struck perpendicular to the rock face, and three MSK23/120 resin coils loaded in each hole. Each steel hinge line is fixed with a steel plate pallet and a QLM type locking device which is matched with the steel hinge line.

The metal mesh is made of cold-drawn steel bars welded together with hooks on both sides of the mesh, a short side and a long side. The full section of the roadway is hung,

the mesh lap length is not less than 100 mm anchor mesh one by one bend hook lap into a whole, mesh hook bend not less than 270°.

After setting anchor ropes and hanging reinforcement network, the roadway is sprayed with initial spraying, with a thickness of 30–50 mm, and then C20 concrete is sprayed to a design thickness of 100 mm, with a maximum distance of 30 m from the head.

Roadway support material parameters specifications are shown in Table 3.

Table 3. Supporting material.

Support Materials	Material	Specification Size	Parameters	Amount of Material per Meter	
				Unit	Quantity
Anchor rods	Left-handed ribless high-strength rebar	Anchor rods: φ20 × 2500 mm	Distance between rows of anchor rods: 1100 × 1200 mm	Size	12
Anchor cable	Steel stranded wire	Anchor cable: φ21.8 × 6200 mm	Distance between rows of anchor cables: 1100 × 1200 mm	Root	9
Mesh	Metal mesh	1300 × 2000 mm/ Mesh 100	Differential pressure between neighbors 100 mm	Sheet	
Anchoring agent	Resin anchors	MSCK2850 MSCK-12/120		Support Support	24 27
Slurry spraying	Slurry spraying material		C20 concrete	m^3	2.99
	Thin spray material		Thin spray material	m^3	0.102
Hardened concrete	Concrete		Base plate C30 concrete	m^3	1.01

The characteristics of the Gaojiabao coal mine west district auxiliary transportation roadway section table are shown in Table 4. As a pioneering rock roadway, its service period is long, and its general use is of the anchor + anchor cable + reinforcement mesh + slurry spray combined support method for the Gaojiabao coal mine TBM round roadway section design support scheme, as shown in Figures 7 and 8.

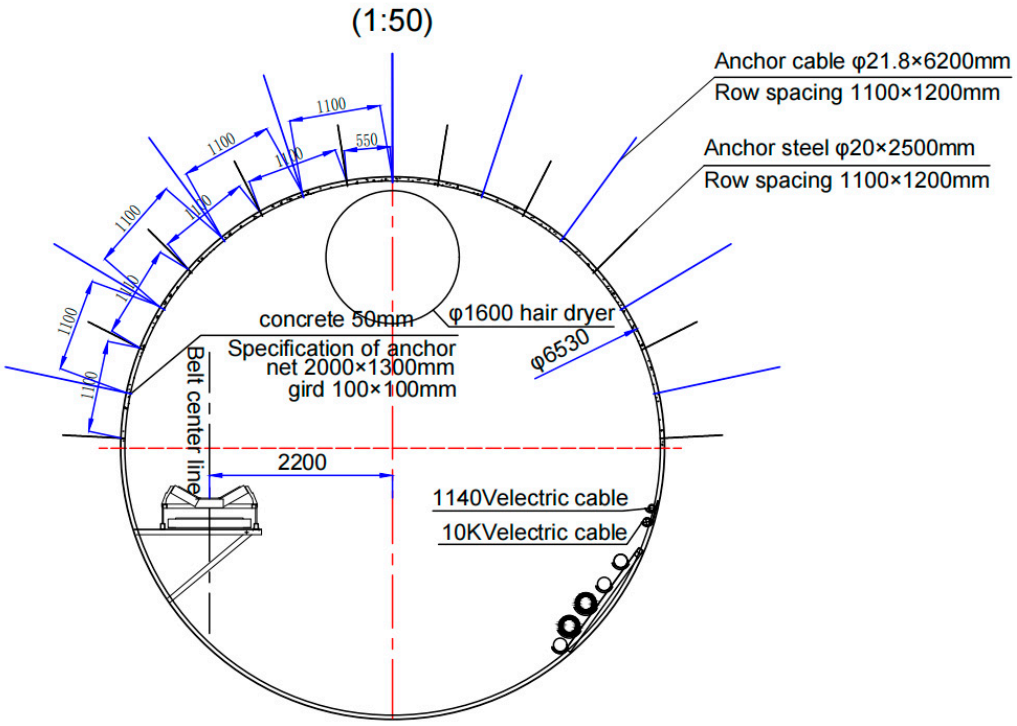

Figure 7. Cross-sectional view of the support scheme.

Table 4. Cross-sectional characteristics of the auxiliary transportation alleys in the west area.

Lane Name	Form of Support	Total Construction Length	Surrounding Rock Hardness	Cross-Section (m^2)		Section Shape	Wilderness Diameter	Spray Thickness (mm)	Strength of Concrete
				Net	Dig				
West District Auxiliary Transport Lane	Anchor network cable spray	4000 m	1~5 (Poor overall performance)	30.47	33.47	Round	6.53 m	150	C20
	Anchor network cable spray	4000 m	1~5 (Good overall performance)	33.27	33.47	Round	6.53 m	10	Spraying materials

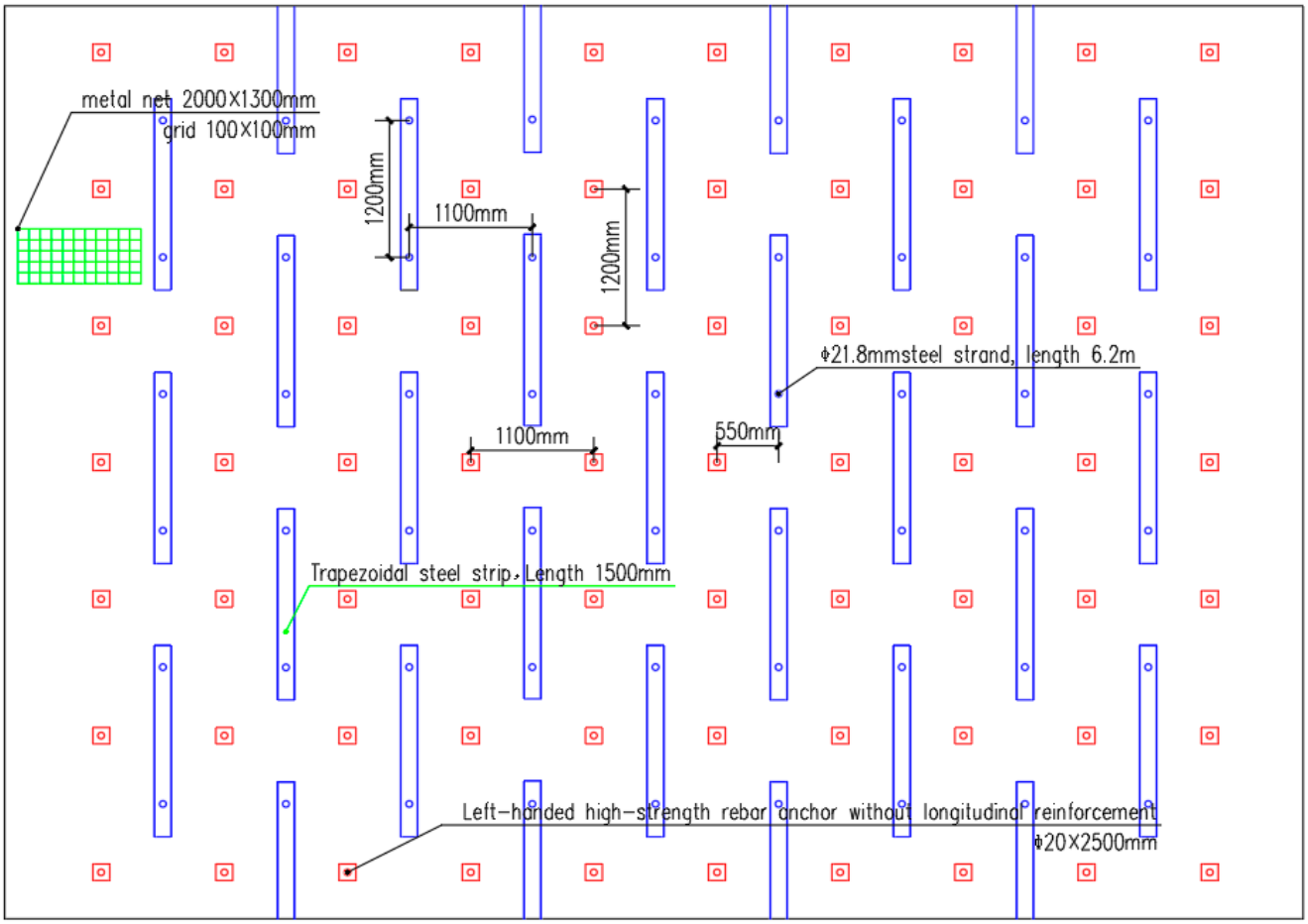

Figure 8. Top view of the support scheme.

4.3. Numerical Simulation Calculation of the Roadway Support

According to the actual production geological conditions of the auxiliary roadway in the west of the Gaojiabao Coal Mine, a numerical simulation model was established to analyze the stability of the surrounding rock of the roadway under different lithologies. Because the roadway is basically not affected by mining, and for the convenience of calculation, the length × width × height of the model built this time was 100 m × 1 m × 100 m, the periphery and bottom of the model were constrained by fixed displacement, the roof was the stress boundary, the vertical pressure was 20 MPa according to the unbuilt rock load γH, and the lateral pressure was 1.8. The model adopted Mohr–Coulomb strength criterion, considered the ultimate failure area under unloading, and did not consider the supporting state.

Taking the roadway arrangement in the medium-grained sandstone layer as an example, the support effect of the roadway was simulated. The anchor rods were Φ22 × 2500 mm, 10 rows each; the inter-row distance was 1100 × 1200 mm, and each anchor rod was anchored by 2 MSK2850 resin anchoring agents. The anchor cables were

arranged alternately with the anchor rods, 9 rows each, with an inter-row distance of 1100 × 1200 mm, anchor cable specification of Φ21.8 × 6200 mm, anchor cable line anchor depth of 6000 mm, anchor cable disc specification of 90 × 90 × 8 mm, and anchor cable specification of 90 × 90 × 8 mm. Each anchor cable was anchored with 3 pieces of MSK2850 resin anchor agent.

Figures 9 and 10 show a cloud diagram of the main stress distribution of the support. From the cloud diagram, it can be seen that the stresses in the roadway are symmetrically distributed, mainly concentrated in the top plate and bottom plate of the roadway, and the stress distribution range of the top plate is larger than that of the bottom plate. The plastic zone of the top slab is compressed because of the supporting effect of anchor rod and anchor cable, which further improves the stability of the roadway. The maximum principal stress and the minimum principal stress of the roadway envelope are uniformly distributed along the roadway; the maximum principal stress is 26.07 MPa and the minimum principal stress is 16.58 MPa.

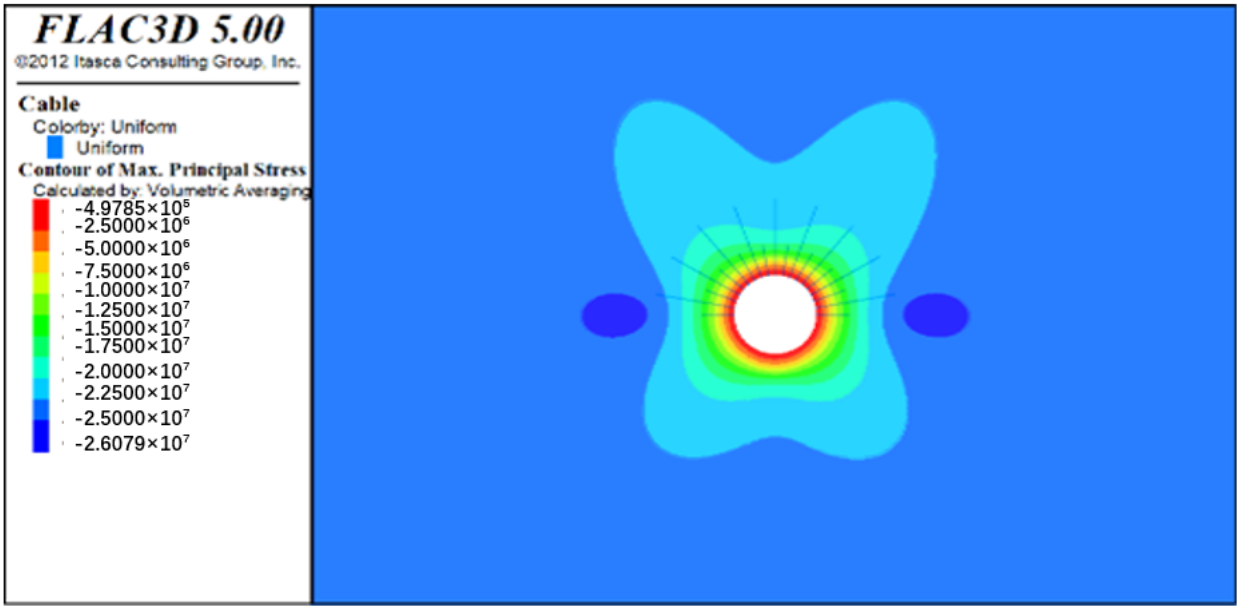

Figure 9. Maximum principal stress distribution cloud.

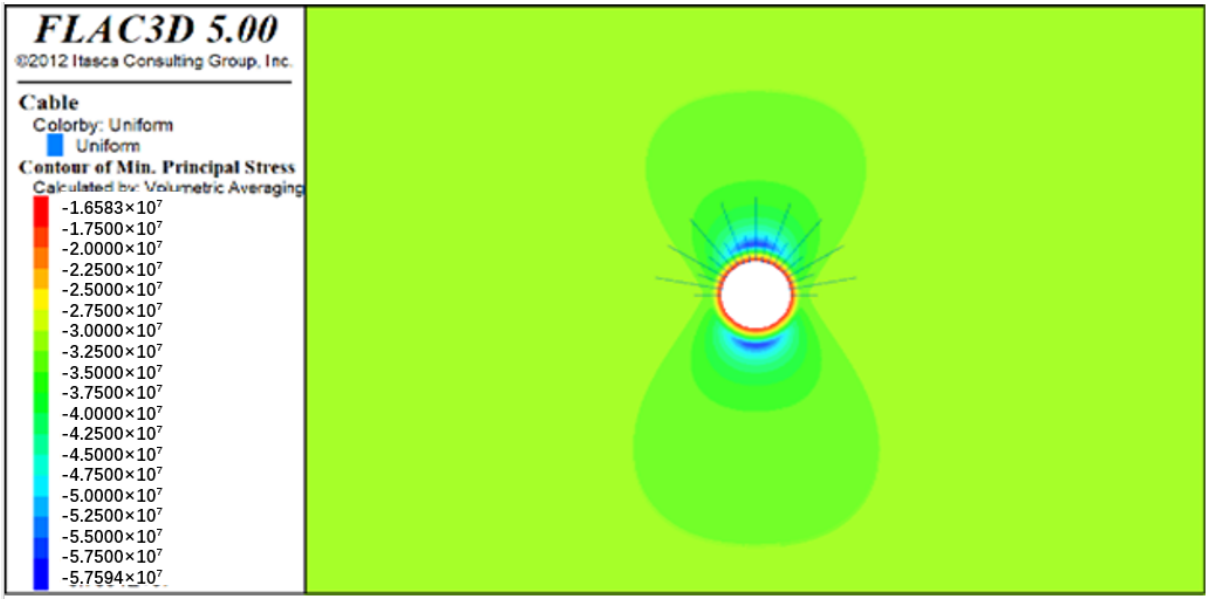

Figure 10. Minimum principal stress distribution cloud.

Figures 11 and 12 shows the displacement distribution of the roadway support rock. From the figure it can be seen that the range of the deformation and damage of the roadway surrounding rock was not large. The deformation and damage of the roadway top plate was of the "pot lid"-type change. The deformation and damage of the roadway center line at the largest range to the two helpers on the extension of the deformation amount gradually reduced. The shallow deformation range was large, and the deep deformation range was small. The bottom plate deformation and damage was of the "anti-pot cover"-type change, and the deformation and damage form and top plate were the same. The maximum deformation of the top plate was 23.9 mm, the maximum deformation of the two sides was 23.3 mm, and the maximum deformation of the bottom plate was 13.8 mm.

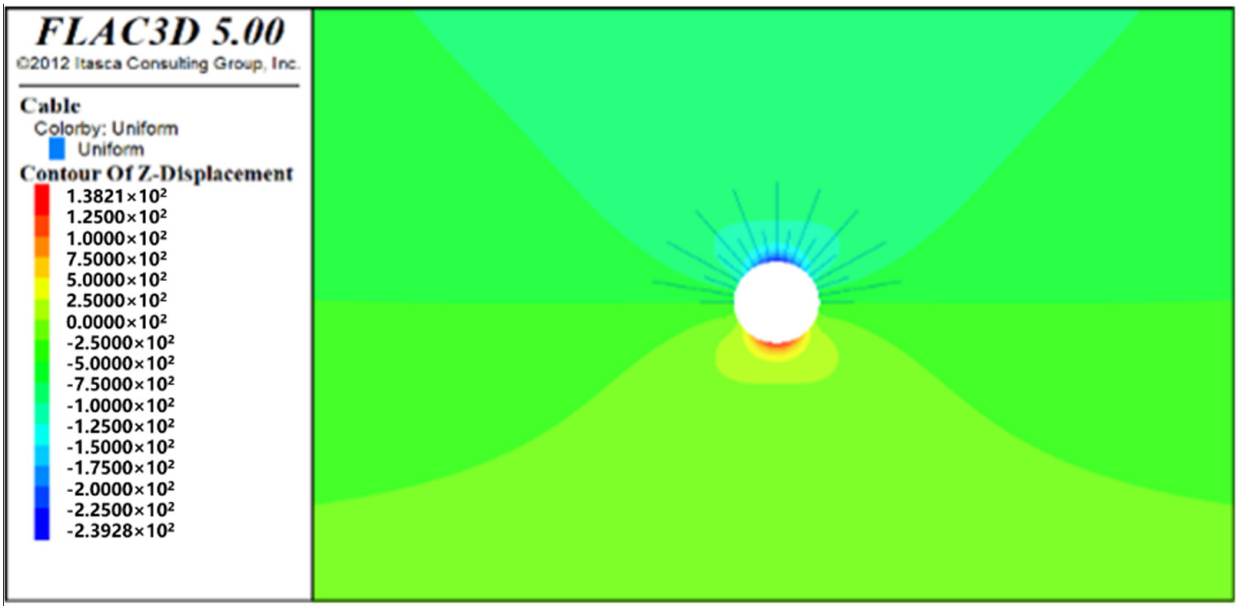

Figure 11. Cloud map of the vertical displacement distribution.

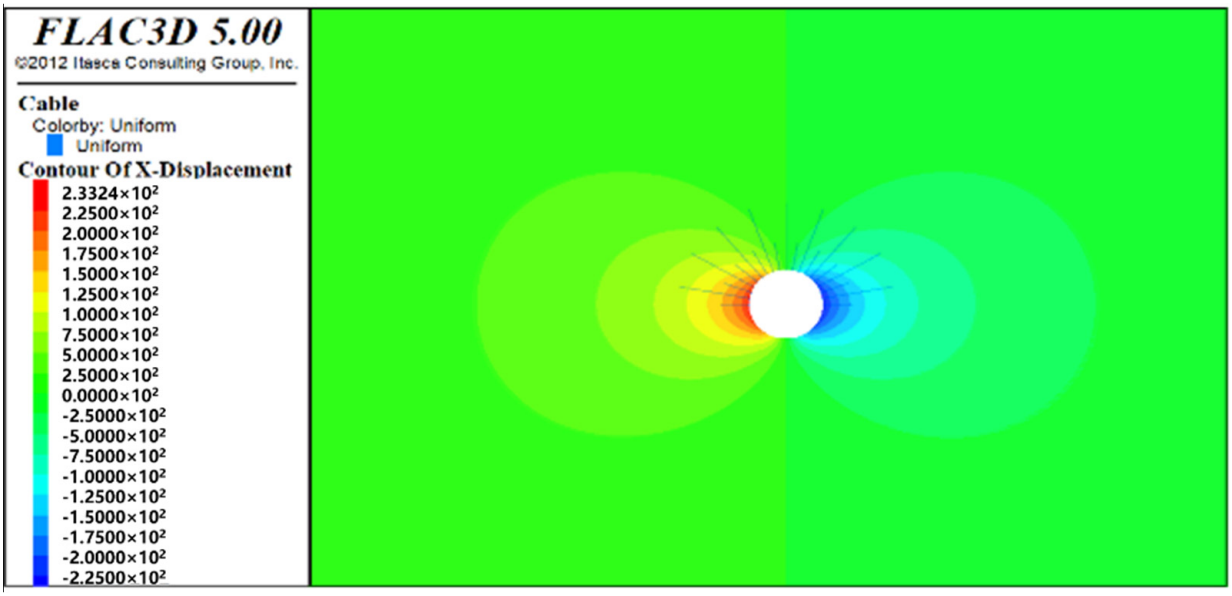

Figure 12. Horizontal displacement distribution cloud map.

5. TBM Intelligent Tunneling Support Process

5.1. TBM Intelligent Tunneling Section Support Process

5.1.1. Segmental Support Program

As shown in Figure 13, the equipment had two supporting platforms, platform 1# and platform 2#, where platform 1# was located at the rear of the drive and on the main beam in front of the propping shoe, equipped with two HC50 anchor rigs for anchor rod support to ensure timely support of the roof of the roadway exposed by the forward movement of the shield body. Platform 2# was located at the rear of the propping shoe and above the front telescopic cylinder, equipped with two anchor rope drilling rigs HC50, responsible for the remaining anchor rod and anchor rope construction. Two MYT-140/320 hydraulic anchor drilling rigs were used to replace the wind-driven anchor drilling rig when the surrounding rock was too hard or the wind was too pressurized to ensure that the anchor rope support does not lag behind.

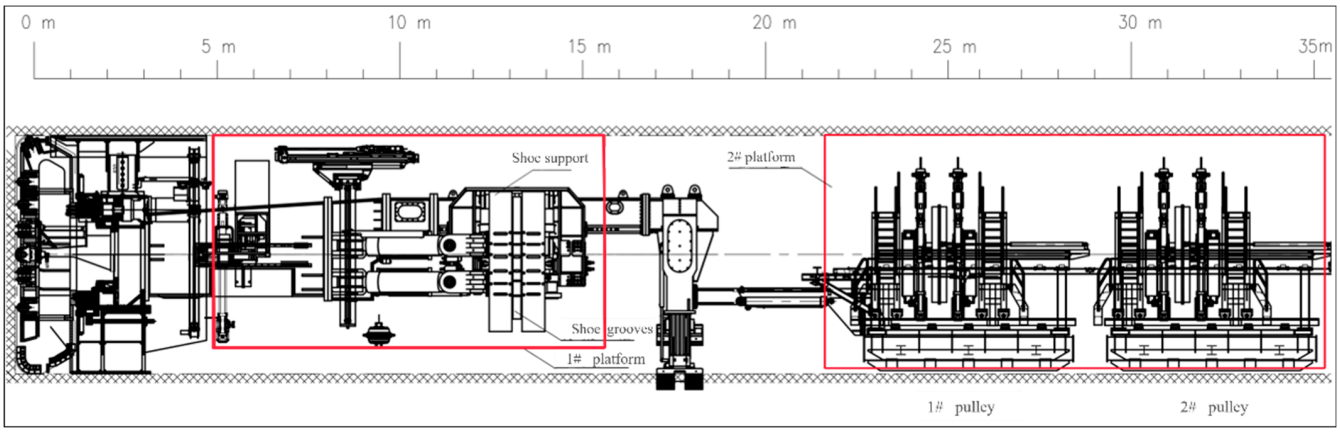

Figure 13. TBM shield machine support part.

The TBM intelligent tunneling subsection support can keep a high daily tunneling record for a long time, which is conducive to achieving the goal of a stable and high yield, and improving the construction efficiency by more than 2~3 times.

5.1.2. Anchor Cable Construction

The open TBM mainframe is symmetrically equipped with four anchor rigs, two of which are located behind the cutter shield and are responsible for drilling anchor rods in the 2 × 120° range at the top of the roadway, while the remaining two are located behind the rear support and are responsible for drilling anchor rods for the roadway patching. The anchor type used is mainly resin anchor, using resin anchor fixing agent to fix the anchor rods. The anchor rods are selected according to the design requirements, corresponding to the surrounding rock level in terms of anchor rod type, length, and spacing, and the construction of the anchor drilling rig is shown in Figure 14.

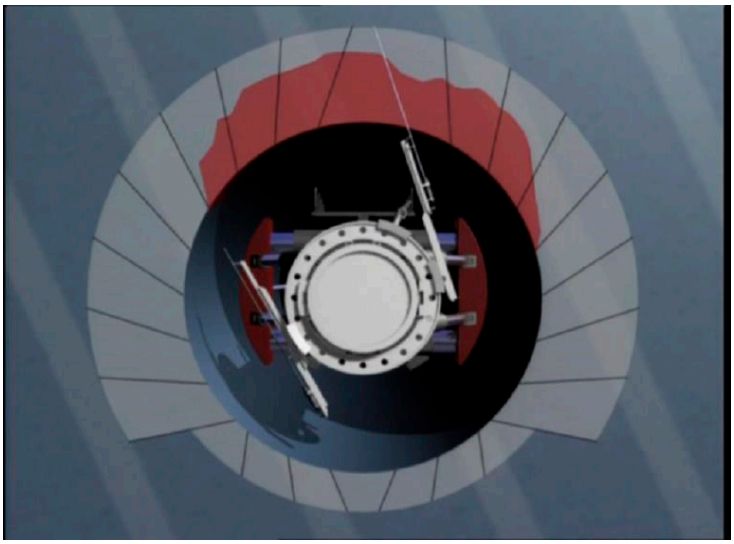

Figure 14. Schematic diagram of anchor construction.

5.2. Reinforcing Mesh and Braided Mesh Installation Process

After each cut, under the cover of temporary support, the top metal net is firstly connected with the top metal net of the previous cycle one by one according to the regulations, and the connection hook is not less than 270°. According to the order from outside to inside, first up and then down, the net is hung and connected in turn. The full section of the mesh is laid close to the rock face, and the connection is made by bending hooks on both sides with a connection length of 100 mm.

The reinforcing mesh is installed in the corresponding rock area according to the design support parameters. The reinforcing mesh is firmly connected to the anchor rod (or steel frame). To prevent the reinforcing mesh from being pulled away from the rock surface by excessive force during the later injection concrete, it must be locally reinforced with coiled bars within the hanging range, and the lap length between two groups of reinforcing mesh is 1 to 2 grids.

5.3. Steel Belt Support Process

The full-round steel frame is installed using the TBM's own steel frame installer (Figure 15). During construction, the machined steel frame is delivered to the arch installer location, the steel frame is connected in sections and the installer is rotated until the next section of the arch can be bolted to the end of the previous section, and the process is repeated until the entire ring is completed, completing the steel arch installation (Figure 16).

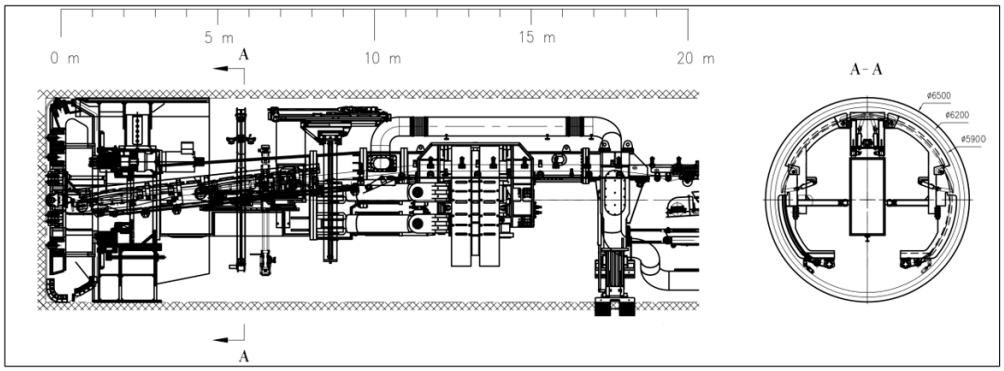

Figure 15. TBM steel frame mounter.

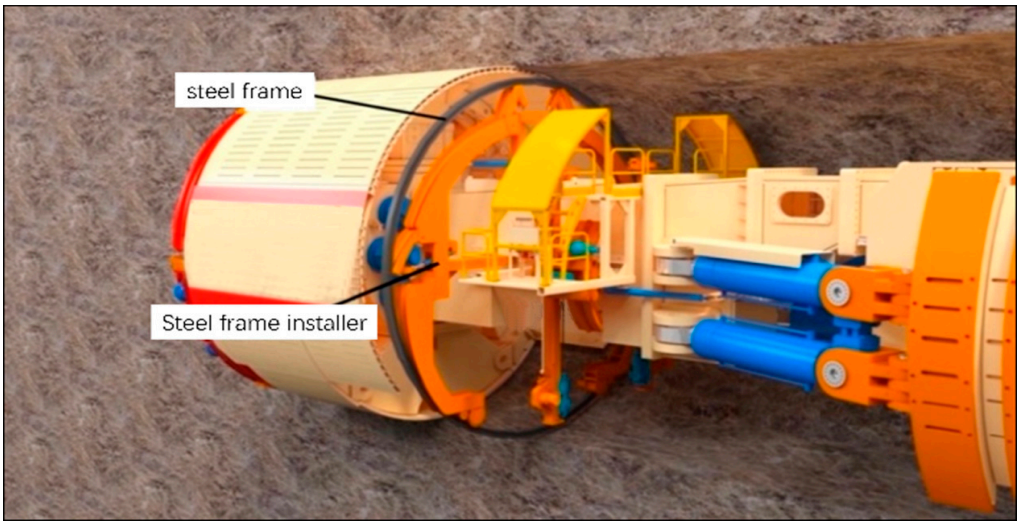

Figure 16. Schematic diagram of steel frame installation.

5.4. Sprayed Concrete Support Process

The concrete is sprayed by the TBM's own spraying system. The concrete is sprayed with the wet spraying method, mixed with liquid alkali-free quicklime, as shown in Figure 17. Spraying concrete from the bottom up, layered operations, quick-setting agent admixture of 3% to 5%, with water lots can be increased. Spraying concrete operations must be followed up in a timely manner, and it is strictly forbidden to tractor after supporting the forward movement of the construction range without completing the spraying operation.

Figure 17. Schematic diagram of sprayed concrete support.

TBM construction will only produce a small amount of dust during excavation, which is beneficial to protect the environment and the health of construction workers.

5.5. Elevation Arch Construction and Rail Line Laying

5.5.1. Installation of Elevated Arch Block

The elevation arch block is prefabricated in the plant and then transported to the installation position for installation. When installing, the supine arch block is close to the previous one, and the width of the gap between the left and right joints is kept consistent and not more than 8 mm. After the supine arch block is installed to the design centerline and elevation, the hook is put down, the chain is released, and the lifting is finished. After the installation of the supine arch block, the allowable deviation is shown in Table 5.

Table 5. Allowable deviation of inverted arch block installation.

Serial Number	Projects	Allowable Deviation (mm)
1	Midline	±20
2	Elevation	±10

5.5.2. Backfill Grouting at the Bottom of the Supine Arch

In general, after laying every 5–6 supine arch blocks, a backfill grouting operation is carried out, and the grouting material is transported from outside the cave to the location of the transfer pump, the grouting pipeline is extended to the installation area of the inverted arch block, and the end of the pipeline is provided with a grouting joint, which is directly inserted into the grouting hole on the inverted arch block for grouting. The grouting material is C20 fine stone concrete, and the grouting pressure is 0.3~0.4 MPa [42,43].

5.5.3. Transport Track Laying

The cave transportation adopts single line rail transportation, the rail is fixed to the elevated arch block through the pre-buried bolts on the elevated arch block, the rail will be backed up to the elevated arch block laying position after unloading the rail, plus the pressure plate, fasteners, and nuts and other fixed accessories, the rail is fixed to complete.

6. Conclusions

(1) Based on the design of TBM tunneling support for complex geological conditions in Gaojiabao coal mine of Shaanxi Zhengtong coal industry, based on the anchorage support design theory and the characteristics of TBM tunneling process, the damage law of the plastic zone of the tunnel surrounding rock under the conditions of different lateral pressure coefficients is studied, and the maximum damage radius of the plastic zone of the tunnel surrounding rock under the conditions of different stress conditions and different lithological combinations of strata is analyzed and determined.

(2) By combining theoretical calculation and numerical simulation, we analyzed and designed the support parameters for the excavation of the west zone pioneer road, the maximum principal stress of the surrounding rock of the roadway is 26.07 MPa, and the minimum principal stress is 16.58 MPa; the maximum deformation of the top plate of the roadway is 23.9 mm, the maximum deformation of the two sides is 23.3 mm, and the maximum deformation of the top plate is 13.8 mm. We proposed a design plan for the support parameters for the excavation of the west zone auxiliary transportation road of 1200 mm, the anchor cable diameter is Φ21.8 mm, length is 6200 mm, row distance is 1100 mm, and spacing is 1200 mm, forming a reasonable support parameter for a large section hard rock roadway for TBM tunneling.

(3) The TBM intelligent tunneling segmental support process, reinforcement mesh and braided mesh installation process, steel belt support process, shotcrete support process, elevation arch construction, and rail line laying, etc., are proposed to correspond

to the field practice, which effectively improve the tunneling efficiency and reduce the economic cost.

(4) In the next step, Zhengtong Coal Company should strengthen the optimization of the adaptability of the equipment structure and the upgrading of the information intelligence, improve the construction process and reasonable production organization and adaptability of the equipment to improve the speed of digging.

Author Contributions: Conceptualization, T.H. and Z.X.; methodology, investigation, and data curation, T.H., L.Z., G.C., Z.D., H.Q. and Y.L.; writing—original draft preparation, T.H.; writing—review and editing, Z.X. and L.Z.; supervision and project administration, Z.D.; funding acquisition, H.Q. and Y.L. All authors have read and agreed to the published version of the manuscript.

Funding: This work was supported and financed by the Natural Science Fund (No. 52074209,51904225), the Natural Science Foundation of Shaanxi Province (No.2021JLM-06), and the Construction of "Scientists + Engineers" Team in Qin Chuangyuan, Shaanxi Province (2023KXJ-057), all of which are greatly appreciated.

Data Availability Statement: The data presented in this study are available upon request from the corresponding author.

Conflicts of Interest: The authors declare that there is no conflicts of interests regarding the publication of the article titled "TBM Rapid Tunneling Roadway Support Parameters Design and Process Research".

References

1. He, F.; Lu, Y.Q.; Dai, E.H.; Tian, Y.Z.; Wu, F.; Pan, S.C.; Zhang, S.; Chen, Z. Coal mine rock tunnel TBM adaptability and new technology development. *Coal Sci. Technol.* **2023**, 1–13. [CrossRef]
2. Cheng, T.L.; Yao, M. Application and development of TBM in coal mine construction. *Eng. Technol. Res.* **2022**, *7*, 115–117. [CrossRef]
3. Wang, D.J.; He, F.; Wang, Y.; Jin, L.J.; Zhao, X.F. Coal mine rock tunneling machine (TBM) and intelligent key technology. *J. Coal* **2020**, *45*, 2031–2044. [CrossRef]
4. Hong, K.R.; Du, Y.L.; Chen, F. Development history, achievements and prospects of full-section tunnel boring machines in China. *Tunn. Constr. (Engl. Chin.)* **2022**, *42*, 739–756.
5. Li, J.B. Current status, problems and prospects of roadheader development in China. *Tunn. Constr. (Chin. Engl.)* **2021**, *41*, 877–896.
6. Liu, Q.S.; Huang, X.; Gong, Q.M.; Du, L.J.; Pan, Y.C.; Liu, J.P. Application and development of hard rock TBM and its prospect in China. *Tunn. Undergr. Space Technol. Inc. Trenchless Technol. Res.* **2016**, *57*, 33–46. [CrossRef]
7. Zhang, H.W.; Hu, Z.F.; Cheng, J.Y.; Zhu, C.Q.; Zhao, Y.X.; Zheng, X.B.; Lv, C.G.; Gao, X.; Zhou, J. Intelligent TBM tunneling technology for large section rock tunnel in deep high-temperature mines: The example of "New Mine No.1". *TBM J. Coal* **2021**, *46*, 2174–2185. [CrossRef]
8. Lv, X.B.; Wang, L.D.; Hao, D.H. Application practice of mining TBM full-section hard rock boring machine with large slope and fast digging turn. *Inn. Mong. Coal Econ.* **2022**, *6*, 147–149. [CrossRef]
9. Yang, S.H.; Rui, F.; Jiang, W.L.; Zhang, S.H. Development and application of full-section rock tunneling machine for coal mines. *Coal Sci. Technol.* **2019**, *47*, 1–10. [CrossRef]
10. Tian, K.X. Research on the construction application of TBM full-section roadheading machine in underground coal mine tunnels. *Contemp. Chem. Res.* **2019**, *43*, 141–142.
11. Tang, B.; Tang, Y.C.; Zhao, N.; Wang, Y.P.; Cao, W.; Bao, B.B.; Wang, Y.G.; Sun, C.H.; Wang, X.Y. Coal mine micro TBM and its digging gas management tunnel engineering practice. *Coal Sci. Technol.* **2023**, 1–9. [CrossRef]
12. Zhou, Z.L.; Dong, J.P.; Wang, S.F.; Cai, X.; Zhou, K. Typical rock-breaking problems and countermeasures in hard rock tunnel TBM construction. *Chin. J. Nonferrous Met.* **2023**, 1–24.
13. Ding, Z.W.; Li, X.F.; Huang, X.; Wang, M.B.; Tang, Q.B.; Jia, J.D. Feature extraction, recognition, and classification of acoustic emission waveform signal of coal rock sample under uniaxial compression. *Int. J. Rock Mech. Min. Sci.* **2022**, *160*, 105262. [CrossRef]
14. Qiu, H.F.; Zhang, F.S.; Liu, L.; Huan, C.; Hou, D.Z.; Kang, W. Experimental study on acoustic emission characteristics of cemented rock-tailings backfill. *Constr. Build. Mater.* **2022**, *315*, 125278. [CrossRef]
15. Ko, T.Y.; Kim, T.K.; Son, Y.; Jeon, S. Effect of geomechanical properties on Cerchar Abrasivity Index (CAI) and its application to TBM tunnelling. *Tunn. Undergr. Space Technol. Inc. Trenchless Technol. Res.* **2016**, *57*, 99–111. [CrossRef]
16. Tang, B.; Cheng, H. Application of Distributed Optical Fiber Sensing Technology in Surrounding Rock Deformation Control of TBM-Excavated Coal Mine Roadway. *J. Sens.* **2018**, *2018*, 1–10.
17. Andy, W. Towards a Mineral Systems Model for Surficial Uranium Mineralization Based on Deposits in the Erongo District of Namibia. *Minerals* **2023**, *13*, 149.

18. Luo, H.Y.; Liang, S.; Yao, Q.L.; Hao, Y.S.; Li, X.H.; Wang, F.R.; Chen, X.Y.; Yang, M. Mechanism and Application of Hydraulic Fracturing in the High-Level Thick and Hard Gangue Layer to Improve Top Coal Caving in Fully Mechanized Caving Mining of an Ultra-Thick Coal Seam. *Minerals* **2022**, *12*, 1605. [CrossRef]
19. Hu, B.; Zhang, C.X.; Zhang, X.Y. The Effects of Hydrochloric Acid Pretreatment on Different Types of Clay Minerals. *Minerals* **2022**, *12*, 1167. [CrossRef]
20. Du, K.; Li, X.B.; Liu, K.W.; Zhao, X.X.; Zhou, Z.L.; Dong, L.J. Comprehensive method and engineering application of goaf risk assessment. *J. Cent. South Univ. (Nat. Sci. Ed.)* **2011**, *42*, 2802–2811.
21. Yang, C. Evaluation of the Effect of Anchor Support in Coal Tunnel and Optimization Design of Reasonable Support Parameters. Master's Thesis, Xi'an University of Science and Technology, Xi'an, China, 2010.
22. Yue, C.Y. Optimization design of support for 2107 track lane in Xinqiao coal mine. *Energy Environ. Prot.* **2018**, *40*, 208–212+217. [CrossRef]
23. Li, P. Optimal design and numerical simulation analysis of roadway support parameters. *Energy Environ. Prot.* **2021**, *43*, 197–201. [CrossRef]
24. Han, T.M. Design and optimization analysis of roadway support parameters. *Mach. Manag. Dev.* **2020**, *35*, 53–54+90. [CrossRef]
25. Zhao, P.P.; Zhao, X.Z.; Liu, Q.; Lu, J.P.; Wang, H.H. Optimization of rapid excavation support parameters for large section coal tunnel. *Mod. Min.* **2022**, *38*, 114–118.
26. Hou, J.S. Optimization study of fast boring support parameters of 31506 semi-coal rock road in Liangzhuang mine. *Coal* **2016**, *25*, 56–58.
27. Ye, H.J. Research on optimization of coal mine roadway support parameters and rapid excavation technology. *Energy Environ. Prot.* **2020**, *42*, 220–223. [CrossRef]
28. Li, X.F. Research on optimization design of coal mine roadway support scheme and support parameters. *Energy Environ. Prot.* **2019**, *41*, 127–130. [CrossRef]
29. Lv, Z.H.; Yang, D.H.; Wang, D. Numerical optimization of anchor support parameters for rapid roadway excavation. *J. Shanxi Datong Univ. (Nat. Sci. Ed.)* **2016**, *32*, 61–65+68.
30. Zhang, X.W.; Duan, Q.T.; Xu, Q.Q. Research on rapid tunneling process and parameter optimization of large section coal tunnel. *China Coal* **2014**, *40*, 87–91+95.
31. Wang, Y.N. Optimization of construction process of tunneling roadway over fault. *Shandong Coal Sci. Technol.* **2022**, *40*, 68–70.
32. Wang, H.W. Research on optimization of construction process and measures for rapid coal tunneling. *Shandong Coal Sci. Technol.* **2018**, *213*, 23–24+26.
33. Cai, F.Y. Optimization design of rapid excavation construction process of No.5 coal seam in Yongdingzhuang coal mine. *Shanxi Sci. Technol.* **2016**, *31*, 156–159.
34. Ren, Z.Z. Optimization of construction process of large section roadway support and rapid tunneling. *Mach. Manag. Dev.* **2022**, *37*, 70–72. [CrossRef]
35. Zhao, J.B. Optimization of construction process of roadway excavation under complex conditions. *Shandong Coal Sci. Technol.* **2019**, *228*, 23–24+27.
36. Du, P.C. Research and application of optimization of fast tunneling construction process of coal tunnel in Sanjiaoxhe mine. *Coal Chem. Ind.* **2019**, *42*, 16–19. [CrossRef]
37. Yue, L. Study on the optimization of construction process of large section boring in Xuan coal Jiaojiazhai mine. *Min. Equip.* **2020**, *111*, 72–73.
38. Zhong, X.Y. Research on optimization of construction process and measures for rapid coal tunneling. *Henan Sci. Technol.* **2021**, *40*, 56–58.
39. Zhang, G.J.; Zhang, Y. Zonal failure characteristics of rock materials under loading (unloading) based on Mohr-Coulomb criterion. *J. Coal Sci.* **2019**, *44*, 1049–1058. [CrossRef]
40. Kang, H.P.; Jiang, T.M.; Gao, F.Q. Design parameters of prestressed anchor support. *Coal J.* **2008**, *7*, 721–726.
41. Dai, J.; Guo, X.S. Parameter optimization of anchor support in coal mine roadways. *Geotechnics* **2009**, *30*, 140–143. [CrossRef]
42. Liu, W.; Liang, J.; Xu, T. Tunnelling-induced ground deformation subjected to the behavior of tail grouting materials. *Tunn. Undergr. Space Technol.* **2023**, *140*, 105253. [CrossRef]
43. Xie, X.; Yang, Y.; Ji, M. Analysis of ground surface settlement induced by the construction of a large-diameter shield-driven tunnel in Shanghai, China. *Tunn. Undergr. Space Technol.* **2016**, *51*, 120–132. [CrossRef]